Computers and Mathematics with Applications 66 (2013) 472–489

Contents lists available at SciVerse ScienceDirect

Computers and Mathematics with Applications

journal homepage: www.elsevier.com/locate/camwa

Numerical simulations of three-dimensional MHD stagnation-point flow of a micropolar fluid

Alessandra Borrelli, Giulia Giantesio *, Maria Cristina Patria

Dipartimento di Matematica e Informatica, Università di Ferrara, via Machiavelli 35, 44121 Ferrara, Italy

ARTICLE INFO

Article history:
Received 24 May 2012
Received in revised form 7 December 2012
Accepted 27 May 2013

Keywords:
Micropolar fluids
MHD flow
Three-dimensional stagnation-point flow
Numerical solutions

ABSTRACT

In this paper the steady three-dimensional stagnation-point flow of an incompressible, homogeneous, electrically conducting micropolar fluid over a flat plate is numerically investigated. The fluid is permeated by a uniform external magnetic field $\mathbf{H}_0$. The effects of the magnetic field on the velocity and on the microrotation profiles are presented graphically and discussed. The results obtained indicate that the thickness of the boundary layer decreases when the magnetic field increases. Moreover $\mathbf{H}_0$ tends to prevent the occurrence of the reverse flow and of the reverse microrotation.

1. Introduction

The three-dimensional stagnation-point flow occurs when a jet of fluid impinges on a rigid body. This is an important example of flow where the three velocity components appear.

This motion has been object of many investigations starting from the paper of Homman in 1936 [1–3]. Through similarity transformations, the study of such a flow is reduced to a non-linear ordinary differential boundary value problem. The obtained system depends upon a parameter $c > -1$ which is a measure of three-dimensionality.

The aim of this paper is to complete our previous analysis concerning the steady three-dimensional flow of an incompressible, homogeneous, electrically conducting micropolar fluid permeated by a uniform external magnetic field $\mathbf{H}_0$ near a three-dimensional stagnation-point of a rigid wall [4]. The coordinate axes are so fixed that the stagnation-point is the origin and that the rigid wall coincides with the plane $x_2 = 0$.

We notice that our results continue to hold even if the obstacle is the surface of a body with any shape, because near the stagnation-point the body may be represented by its tangent plane (the plane $x_2 = 0$).

The micropolar fluids introduced by Eringen [5] physically represent fluids consisting of rigid randomly oriented particles suspended in a viscous medium which have an intrinsic rotational micromotion (for example biological fluids in thin vessels, polymeric suspensions, slurries, colloidal fluids). Extensive reviews on the theory and its applications can be found in [5,6]. We remark that, in recent years a vast amount of literature concerning the analytical solutions of flow of a micropolar fluid is available [7–10]. Moreover many papers concerning the applications and numerical simulations have been published [11–19]. We underline that in most of the studies in the literature a restrictive approach has been followed on the material parameters which make the equations to contain only one parameter [20], while in our research we do not require restrictive conditions so that three material parameters appear in the dimensionless ODEs.

This paper completes the study concerning the micropolar fluids developed in [4], where we have proved that, if an external magnetic field $\mathbf{H}_0$ is impressed, and the induced magnetic field is neglected (as it is customary when the magnetic

* Corresponding author. Tel.: +39 3349016305.
E-mail addresses: brs@unife.it (A. Borrelli), giulia.giantesio@unife.it, gntgli@unife.it (G. Giantesio), pat@unife.it (M.C. Patria).

0898-1221/$ – see front matter © 2013 Elsevier Ltd. All rights reserved.
http://dx.doi.org/10.1016/j.camwa.2013.05.023

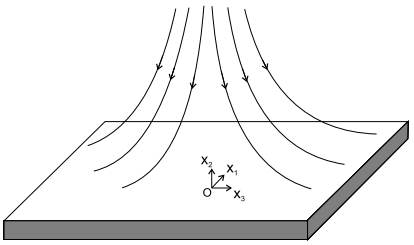

Fig. 1. Flow description.

Reynolds number is very small), then the steady three-dimensional MHD stagnation-point flow is possible if, and only if, $\mathbf{H}_0$ has the direction of one of the coordinate axes.

By means of similarity transformations, we find that the flow has to satisfy a non-linear ordinary differential boundary value problem whose form depends on the direction of $\mathbf{H}_0$. The solutions of the three problems depend on $\mathbf{H}_0$ through the Hartmann number M^2.

In this paper we solve the boundary value problems by numerical integration, because they are not solvable in closed form due to non-linearity.

We underline that if $M^2 = 0$, then the systems we find reduce to the system governing the flow of a micropolar fluid in the absence of the magnetic field [21], while the results for $M^2 \neq 0$ are totally new. Moreover our results for $M^2 = 0$ extend the previous one contained in [21], where, the Authors did not take into consideration the occurrence of the reverse flow, the thickness of the boundary layer and the influence of some parameters on the solution.

Thanks to the numerical integration, in the three cases, in addition to the well known phenomenon of the reverse flow, we find a new interesting result: the microrotation presents a zone of reverse microrotation for some negative values of c. The range of c for which the reverse microrotation appears is included in the range of c for which the reverse flow occurs. Further we find that $\mathbf{H}_0$ tends to prevent the occurrence of the reverse flow and the occurrence of the reverse microrotation.

The presence of $\mathbf{H}_0$ modifies also the thickness of the boundary layer which decreases as M^2 increases. This effect occurs in all cases studied and it is standard in MHD.

Finally, it is interesting to compare these results with the corresponding results for the Newtonian fluids [22]: in particular the micropolar fluids reduce the thickness of the boundary layer, the magnitude of the skin friction, and the negative value of c for which the reverse flow does not occur starting from $M^2 = 0.2$ (CASEs I–II).

The paper is organized in this way:

in Section 2, we formulate the problem, and recall the results contained in [4].

In Section 3, we integrate numerically the previous problems, and discuss the physics of the results obtained.

Section 4 is devoted to conclusions.

2. Overview of the problem

In [4] we have studied the steady three-dimensional MHD stagnation-point flow of an incompressible homogeneous electrically conducting micropolar fluid towards a flat surface. We assume that the flat surface is the rigid, fixed, non-electrically conducting wall of equation $x_2 = 0$, so that the flow is confined to the half-space $\mathcal{S} = \{(x_1, x_2, x_3) \in \mathbb{R}^3 : (x_1, x_3) \in \mathbb{R}^2, x_2 > 0\}$ (see Fig. 1).

We recall that in the absence of external mechanical body forces and body couples, the MHD equations for such a fluid are [6]

$$\begin{aligned}
&\mathbf{v}\cdot\nabla\mathbf{v} = -\frac{1}{\rho}\nabla p + (\nu+\nu_r)\triangle\mathbf{v} + 2\nu_r(\nabla\times\mathbf{w}) + \frac{\mu_e}{\rho}(\nabla\times\mathbf{H})\times\mathbf{H},\\
&\nabla\cdot\mathbf{v} = 0,\\
&I\mathbf{v}\cdot\nabla\mathbf{w} = \lambda\triangle\mathbf{w} + \lambda_0\nabla(\nabla\cdot\mathbf{w}) - 4\nu_r\mathbf{w} + 2\nu_r(\nabla\times\mathbf{v}),\\
&\nabla\times\mathbf{H} = \sigma_e(\mathbf{E} + \mu_e\mathbf{v}\times\mathbf{H}),\\
&\nabla\times\mathbf{E} = \mathbf{0}, \qquad \nabla\cdot\mathbf{E} = 0, \qquad \nabla\cdot\mathbf{H} = 0, \quad \text{in } \mathcal{S}
\end{aligned} \tag{1}$$

where $\mathbf{v}$ is the velocity field, $\mathbf{w}$ is the microrotation field, p is the pressure, $\mathbf{E}$ and $\mathbf{H}$ are the electric and magnetic fields, respectively, ν is the kinematic Newtonian viscosity coefficient, ν_r is the microrotation viscosity coefficient, λ, λ_0 (positive constants) are material parameters related to the coefficients of angular viscosity, I is the microinertia coefficient, ρ is the mass density (constant >0), μ_e is the magnetic permeability, and σ_e is the electrical conductivity (μ_e, σ_e = constants > 0).

As it is well known, the three-dimensional stagnation-point flow is described by a velocity field of the form [23]

$$v_1 = ax_1 f'(\eta), \qquad v_2 = -\sqrt{(\nu+\nu_r)a}[f(\eta) + cg(\eta)], \qquad v_3 = cax_3 g'(\eta), \tag{2}$$

and by a microrotation field of the form [21]

$$w_1 = -c\frac{a^2}{2\nu_r}\sqrt{\frac{\nu+\nu_r}{a}}x_3F(\eta), \qquad w_2 = 0, \qquad w_3 = \frac{a^2}{2\nu_r}\sqrt{\frac{\nu+\nu_r}{a}}x_1G(\eta), \tag{3}$$

where a is a positive parameter, c is a constant which is a measure of three-dimensionality, f, g, F, G are sufficiently regular unknown dimensionless functions and $\eta = \sqrt{\frac{a}{\nu+\nu_r}}x_2$.

We exclude in our analysis $c = 0$, because this describes the orthogonal plane stagnation-point flow.

Moreover, the usual adherence condition on the boundary supplies

$$\begin{aligned} &f(0) = 0, \qquad f'(0) = 0, \qquad g(0) = 0, \qquad g'(0) = 0,\\ &F(0) = 0, \qquad G(0) = 0. \end{aligned} \tag{4}$$

As it is customary, we assume that at infinity, the flow approaches the flow of an inviscid fluid impinging on the flat plane $\eta = h$ [4], whose velocity is given by:

$$v_1 = ax_1, \qquad v_2 = -\sqrt{(\nu+\nu_r)a}(1+c)(\eta-h), \qquad v_3 = cax_3, \qquad \eta \geq h. \tag{5}$$

Therefore, to (4) we also must append the following conditions

$$\begin{aligned} &\lim_{\eta\to+\infty} f'(\eta) = 1, \qquad \lim_{\eta\to+\infty} g'(\eta) = 1,\\ &\lim_{\eta\to+\infty} F(\eta) = 0, \qquad \lim_{\eta\to+\infty} G(\eta) = 0. \end{aligned} \tag{6}$$

The constant h in (5) is the three-dimensional displacement thickness [3] and it is related to the behaviour of f and g at infinity. Actually, if

$$\lim_{\eta\to+\infty}[f(\eta)-\eta] = -\alpha, \qquad \lim_{\eta\to+\infty}[g(\eta)-\eta] = -\beta \tag{7}$$

with α, β some constants, then

$$\lim_{\eta\to+\infty}[f(\eta)+cg(\eta)-(1+c)\eta] = -(1+c)h, \tag{8}$$

from which

$$h = \frac{\alpha+c\beta}{1+c}.$$

The constants α, β are not assigned a priori, but their values can be found by solving the problem. As we will see, the three-dimensional displacement thickness h can be positive or negative.

We exclude the case $c \leq -1$ because we impose in (5) the condition $v_2 < 0$, so that the inviscid fluid moves towards the wall $\eta = h$. Hence in the further analysis we assume that $c \in (-1, 0) \cup (0, +\infty)$.

Supposing that a uniform external magnetic field $\mathbf{H}_0$ is impressed and that the electric field is absent, under the hypothesis that the magnetic Reynolds number is very small, so that the induced magnetic field is negligible in comparison with the imposed field, we have proved in [4] the following

Theorem 1. *Let a homogeneous, incompressible, electrically conducting micropolar fluid occupy the half-space $\mathcal{S}$. If we neglect the induced magnetic field, then the steady three-dimensional MHD stagnation-point flow of such a fluid is possible if, and only if, the external magnetic field $\mathbf{H}_0$ is parallel to one of the axes (with unit vector $\mathbf{e}_i$ for $i = 1, 2, 3$). Moreover, the flow has the form (2), (3), $\mathbf{E} = \mathbf{0}$, and*

(I) *if $\mathbf{H}_0 = H_0\mathbf{e}_1$, then (f, g, F, G) satisfies problem*

$$f''' + (f+cg)f'' - f'^2 + 1 + G' = 0,$$

$$g''' + (f+cg)g'' - cg'^2 + c + F' + M^2(1-g') = 0, \tag{9}$$

$$F'' + c_3F'(f+cg) - F(c_3cg' + c_2) - c_1g'' = 0,$$

$$G'' + c_3G'(f+cg) - G(c_3f' + c_2) - c_1f'' = 0, \tag{10}$$

$$\begin{aligned} &f(0) = 0, \qquad f'(0) = 0, \qquad g(0) = 0, \qquad g'(0) = 0,\\ &F(0) = 0, \qquad G(0) = 0,\\ &\lim_{\eta\to+\infty} f'(\eta) = 1, \qquad \lim_{\eta\to+\infty} g'(\eta) = 1,\\ &\lim_{\eta\to+\infty} F(\eta) = 0, \qquad \lim_{\eta\to+\infty} G(\eta) = 0, \end{aligned} \tag{11}$$

where $M^2 = \frac{\sigma_e \mu_e^2 H_0^2}{\rho a}$ *is the Hartmann number and*

$$c_1 = \frac{4\nu_r^2}{\lambda a}, \qquad c_2 = \frac{4\nu_r(\nu+\nu_r)}{\lambda a}, \qquad c_3 = \frac{I}{\lambda}(\nu+\nu_r); \tag{12}$$

(II) *if* $\mathbf{H}_0 = H_0\mathbf{e}_2$, *then* (f, g, F, G) *satisfies problem*

$$\begin{aligned} &f''' + (f+cg)f'' - f'^2 + 1 + G' + M^2(1-f') = 0,\\ &g''' + (f+cg)g'' - cg'^2 + c + F' + M^2(1-g') = 0, \end{aligned} \tag{13}$$

with (10) *and the boundary conditions* (11);

(III) *if* $\mathbf{H}_0 = H_0\mathbf{e}_3$, *then* (f, g, F, G) *satisfies problem*

$$\begin{aligned} &f''' + (f+cg)f'' - f'^2 + 1 + G' + M^2(1-f') = 0,\\ &g''' + (f+cg)g'' - cg'^2 + c + F' = 0, \end{aligned} \tag{14}$$

with (10) *and the boundary conditions* (11).

Remark 2. If $M^2 = 0$, then Eqs. (9) (or (13), or (14)), (10) reduce to equations found by Guram and Anwar Kamal in [21].

Remark 3. We notice that, the pressure field which corresponds to the three cases of Theorem 1 is respectively:

$$\begin{aligned} p = {} & -\rho\frac{a^2}{2}\left\{x_1^2 + \frac{\nu+\nu_r}{a}[f(\eta)+cg(\eta)]^2 + c^2x_3^2\right\} - \rho a(\nu+\nu_r)[f'(\eta)+cg'(\eta)]\\ & - 2\nu_r\rho\frac{\nu+\nu_r}{a}\int_0^\eta [cF(s)+G(s)]ds + \rho a^2M^2\left\{\frac{\nu+\nu_r}{a}\int_0^\eta [f(s)+cg(s)]ds - \frac{c}{2}x_3^2\right\} + p_0, \end{aligned} \tag{15}$$

$$\begin{aligned} p = {} & -\rho\frac{a^2}{2}\left\{x_1^2 + \frac{\nu+\nu_r}{a}[f(\eta)+cg(\eta)]^2 + c^2x_3^2\right\} - \rho a(\nu+\nu_r)[f'(\eta)+cg'(\eta)]\\ & - 2\nu_r\rho\frac{\nu+\nu_r}{a}\int_0^\eta [cF(s)+G(s)]ds - \rho a^2M^2(x_1^2+cx_3^2) + p_0, \end{aligned} \tag{16}$$

$$\begin{aligned} p = {} & -\rho\frac{a^2}{2}\left\{x_1^2 + \frac{\nu+\nu_r}{a}[f(\eta)+cg(\eta)]^2 + c^2x_3^2\right\} - \rho a(\nu+\nu_r)[f'(\eta)+cg'(\eta)]\\ & - 2\nu_r\rho\frac{\nu+\nu_r}{a}\int_0^\eta [cF(s)+G(s)]ds + \rho a^2M^2\left\{\frac{\nu+\nu_r}{a}\int_0^\eta [f(s)+cg(s)]ds - \frac{x_1^2}{2}\right\} + p_0. \end{aligned} \tag{17}$$

It is important to explicit the pressure field because, as we will see in Section 3, if one of the components of the pressure gradient parallel to the wall has the same sign of the corresponding component of the velocity or of the microrotation curl field, then the reverse flow or the reverse microrotation appears.

3. Numerical results and discussion from a physical point of view

In this section, we discuss the numerical solutions of the problems studied in Theorem 1. These numerical solutions are obtained using the MATLAB routine **bvp4c**. Such a routine is a finite difference code that implements the three-stage Lobatto IIIa formula. This is a collocation formula and here the collocation polynomial provides a C^1-continuous solution that is fourth-order accurate uniformly in $[0, 5]$. Mesh selection and error control are based on the residual of the continuous solution. We set the relative and the absolute tolerance equal to 10^{-7}. The method was used and described in [24].

The values of the parameters $c,\ c_1,\ c_2,\ c_3$ are chosen according to [2,3,21]. Of course by virtue of (12), $c_2 > c_1$.

The numerical integration points out some results which are very interesting from a physical point of view.

First of all, we see that the solution (f, g, F, G) of the three problems considered in Theorem 1 satisfies the conditions (6) and (7); therefore we define:

- $\overline{\eta}_f$ $(\overline{\eta}_g)$ the value of η such that $f'(\overline{\eta}_f) = 0.99$ $(g'(\overline{\eta}_g) = 0.99)$;
- $\overline{\eta}_F$ $(\overline{\eta}_G)$ the value of η such that $F(\overline{\eta}_F) = -0.01$ $(G(\overline{\eta}_G) = -0.01)$.

Hence if $\eta > \overline{\eta}_f$ $(\eta > \overline{\eta}_g)$, then $f \cong \eta - \alpha$ $(g \cong \eta - \beta)$, and if $\eta > \overline{\eta}_F$ $(\eta > \overline{\eta}_G)$, then $F \cong 0$ $(G \cong 0)$.

Therefore, the numerical integration shows that the influence of the viscosity on the velocity and on the microrotation appears only in a layer lining the boundary whose thickness is $\delta_v = \max(\overline{\eta}_f, \overline{\eta}_g)$ for the velocity and $\delta_w = \max(\overline{\eta}_F, \overline{\eta}_G)$ for the microrotation. Such a phenomenon is known from the experimental observations.

The thickness δ of the boundary layer for the flow is defined as

$$\delta = \max(\delta_v, \delta_w).$$

Another very significant feature from a physical point of view is the occurrence of the reverse flow and of the reverse microrotation.

This effect is well known for the velocity field of a Newtonian fluid [3,22,25], while the reverse microrotation has never been observed in the literature.

The numerical results show that there exists a negative value c_r of c such that if $c \geq c_r$, then $g', g'' > 0\ \forall \eta > 0$, and if $c < c_r$ then near the wall $g', g'' < 0$, so that the reverse flow appears (i.e. v_3 has the same sign of $\frac{\partial p}{\partial x_3}$). Moreover we have found numerically that there exists a negative value c_{rw} of c such that if $c \geq c_{rw}$, then $F'(0) < 0, F(\eta) < 0\ \forall \eta > 0$, and if $c < c_{rw}$ then near the wall $F, F' > 0$ so that the reverse microrotation appears (i.e. $(\nabla \times \mathbf{w})_3 = \frac{a^2}{2\nu_r} c x_3 F'(\eta)$ has the same sign of $\frac{\partial p}{\partial x_3}$). We underline that when the reverse microrotation appears, w_1 is positive if $x_3 < 0$, while it is negative if $x_3 > 0$.

The reverse flow and the reverse microrotation are also related to a sign change of the scalar component of the skin friction ($\tau_{\mathbf{0}}$) in the direction of $\mathbf{e}_3$ and of the scalar component of the skin couple friction ($\gamma_{\mathbf{0}}$) in the direction of $\mathbf{e}_1$:

$$\begin{aligned}\tau_{\mathbf{0}} &= \rho a^{3/2}(\nu + \nu_r)^{1/2}\{x_1[f''(0) + G(0)]\mathbf{e}_1 + c x_3[g''(0) + F(0)]\mathbf{e}_3\} \\ &= \rho a^{3/2}(\nu + \nu_r)^{1/2}[x_1 f''(0)\mathbf{e}_1 + c x_3 g''(0)\mathbf{e}_3],\end{aligned} \tag{18}$$

$$\gamma_{\mathbf{0}} = \rho\lambda\frac{a^2}{2\nu_r}[-c x_3 F'(0)\mathbf{e}_1 + x_1 G'(0)\mathbf{e}_3]. \tag{19}$$

As one can see from (15), (16), (17), the pressure field depends on the external magnetic field through the Hartmann number M^2, which influences the sign of the components of the pressure gradient along the surface. For this reason, as we deduce from the numerical results, the presence of the external magnetic field tends to prevent the occurrence of the reverse flow and of the reverse microrotation. This behaviour appears more clearly in CASEs I–II. The influence of the external magnetic field on the reverse flow has already been observed in [26] for a Newtonian fluid in other physical situations.

Before considering the CASEs I–II–III, it is convenient to examine the three-dimensional stagnation-point flow for a micropolar fluid in the absence of the external magnetic field. Our results are consistent with the previous studies when $M^2 = 0$ [21], where, however, the Authors did not consider the occurrence of the reverse flow and of the reverse microrotation, the thickness of the boundary layer, the parameters α, β, h and the influence of c_1, c_2, c_3 on the solution. Hence our results for $M^2 = 0$ extend and complete the previous one.

In particular when $M^2 = 0$ and $c = 1$ we obtain the $\eta -$ axial symmetric flow: $\alpha = \beta = h, f''(0) = g''(0)$ and $F'(0) = G'(0)$.

3.1. $M^2 = 0$

In Table 1 we display the values of $f''(0), g''(0), F'(0), G'(0), h, \alpha, \beta, \overline{\eta}_f, \overline{\eta}_g, \overline{\eta}_F$ and $\overline{\eta}_G$ when $c,\ c_1,\ c_2,\ c_3$ change and $M^2 = 0$. $f''(0), g''(0), F'(0), G'(0)$ are important for the physics of the problem because they appear in the expression of $\tau_{\mathbf{0}}$ and $\gamma_{\mathbf{0}}$ (see (18) and (19)) and they influence the occurrence of the reverse flow and the reverse microrotation. We recall that h is the three dimensional displacement thickness so that $\eta = h$ is the flat plane towards which the inviscid fluid, whose flow is approached at infinity by the micropolar fluid, impinges. We remark that h can be negative.

From Table 1 it appears that if we fix two parameters among c_1, c_2, c_3, then the influence of c_1 on the descriptive quantities of motion is more evident.

Figs. 2–4 elucidate the dependence of the functions f', g', F, G, on the parameters c_1, c_2, c_3 when $M^2 = 0$. We can see that the functions which appear most influenced by c_1, c_2, c_3 are F and G, in other words the microrotation, as we can expect because this vector characterizes the micropolar fluid. More precisely, the profiles of F and G rise as c_2 or c_3 increase and c_1 decreases; c_1 is the parameter that most influences the microrotation. The other two functions, f' and g', do not show considerable variations as $c_1,\ c_2,\ c_3$ assume different values.

We do not display the graphics of f, g, F, G because they are analogous to those which we will show in the presence of the external magnetic field.

We now consider the influence of the magnetic field. We underline that there are no results in the literature whenever $M^2 \neq 0$.

3.2. Case I: $\mathbf{H}_0 = H_0\mathbf{e}_1$

As we have already seen, the external magnetic field influences directly the velocity through M^2 which appears only in Eq. $(9)_2$.

We have solved problem (9), (10), (11) numerically.

Fig. 5 shows the graphics of f, f', f''.

Table 1
Descriptive quantities of motion for some values of c, c_1, c_2, c_3, and M^2.

M^2	c	c_1	c_2	c_3	$f''(0)$	$g''(0)$	$F'(0)$	$G'(0)$	h	α	β	$\overline{\eta}_f$	$\overline{\eta}_g$	$\overline{\eta}_F$	$\overline{\eta}_G$
0	−0.75	0.1	1.5	0.1	1.2357	−0.4704	−0.0005	−0.0536	−4.9584	0.6343	2.4986	2.3204	4.4516	3.6586	1.5789
				0.5	1.2371	−0.4709	−0.0015	−0.0514	−4.9640	0.6347	2.5009	2.3332	4.4701	3.4224	1.3102
			3.0	0.1	1.2389	−0.4692	0.0050	−0.0448	−5.0094	0.6352	2.5167	2.3424	4.4915	2.8943	0.9930
				0.5	1.2395	−0.4695	0.0046	−0.0438	−5.0111	0.6353	2.5175	2.3486	4.4976	2.7868	0.8370
		0.5	1.5	0.1	1.1916	−0.4715	−0.0123	−0.2680	−4.3976	0.6209	2.2937	2.1157	3.9136	4.5392	2.9134
				0.5	1.1984	−0.4753	−0.0163	−0.2573	−4.4520	0.6225	2.3140	2.1616	4.0678	4.3181	2.4464
			3.0	0.1	1.2082	−0.4694	0.0222	−0.2242	−4.7357	0.6248	2.4116	2.2046	4.2871	4.2340	2.3241
				0.5	1.2112	−0.4708	0.0202	−0.2194	−4.7497	0.6256	2.4173	2.2319	4.3326	4.0645	2.1007
	−0.25	0.1	1.5	0.1	1.2144	0.2605	−0.0289	−0.0529	0.4224	0.6558	1.3558	2.4106	3.5133	2.6648	1.6156
				0.5	1.2156	0.2611	−0.0290	−0.0508	0.4226	0.6560	1.3563	2.4222	3.5366	2.4337	1.3547
			3.0	0.1	1.2176	0.2636	−0.0205	−0.0441	0.4214	0.6566	1.3625	2.4334	3.5658	1.7784	0.9979
				0.5	1.2181	0.2638	−0.0207	−0.0432	0.4215	0.6568	1.3627	2.4387	3.5745	1.6902	0.8452
		0.5	1.5	0.1	1.1705	0.2296	−0.1479	−0.2643	0.4289	0.6414	1.2788	2.1959	3.0656	3.8678	2.9608
				0.5	1.1770	0.2323	−0.1490	−0.2541	0.4294	0.6427	1.2825	2.2389	3.1574	3.4688	2.5088
			3.0	0.1	1.1870	0.2454	−0.1042	−0.2205	0.4228	0.6458	1.3148	2.2932	3.3251	3.3429	2.3762
				0.5	1.1897	0.2462	−0.1051	−0.2160	0.4232	0.6464	1.3160	2.3177	3.3681	3.1414	2.1642
	0.25	0.1	1.5	0.1	1.2369	0.7946	−0.0454	−0.0537	0.6662	0.6263	0.8257	2.2136	2.5693	1.9307	1.5711
				0.5	1.2383	0.7958	−0.0443	−0.0514	0.6664	0.6265	0.8260	2.2241	2.5848	1.6679	1.2934
			3.0	0.1	1.2400	0.7982	−0.0362	−0.0449	0.6671	0.6270	0.8274	2.2319	2.5978	1.2652	1.0015
				0.5	1.2406	0.7986	−0.0359	−0.0439	0.6672	0.6271	0.8275	2.2371	2.6044	1.1405	0.8419
		0.5	1.5	0.1	1.1931	0.7515	−0.2276	−0.2687	0.6514	0.6139	0.8013	2.0329	2.3194	3.1593	2.8349
				0.5	1.2003	0.7576	−0.2227	−0.2575	0.6524	0.6149	0.8027	2.0717	2.3749	2.6586	2.3296
			3.0	0.1	1.2092	0.7698	−0.1817	−0.2247	0.6559	0.6174	0.8099	2.1111	2.4429	2.6063	2.2902
				0.5	1.2124	0.7722	−0.1801	−0.2198	0.6564	0.6179	0.8104	2.1339	2.4727	2.3687	2.0482
	1.00	0.1	1.5	0.1	1.3013	1.3013	−0.0558	−0.0558	0.5665	0.5665	0.5665	1.9071	1.9071	1.4569	1.4569
				0.5	1.3030	1.3030	−0.0531	−0.0531	0.5667	0.5667	0.5667	1.9166	1.9166	1.1527	1.1527
			3.0	0.1	1.3043	1.3043	−0.0470	−0.0470	0.5670	0.5670	0.5670	1.9201	1.9201	0.9782	0.9782
				0.5	1.3051	1.3051	−0.0458	−0.0458	0.5671	0.5671	0.5671	1.9251	1.9251	0.8015	0.8015
		0.5	1.5	0.1	1.2583	1.2583	−0.2793	−0.2793	0.5568	0.5568	0.5568	1.7701	1.7701	2.6108	2.6108
				0.5	1.2669	1.2669	−0.2657	−0.2657	0.5576	0.5576	0.5576	1.8056	1.8056	2.0339	2.0339
			3.0	0.1	1.2734	1.2734	−0.2354	−0.2354	0.5594	0.5594	0.5594	1.8246	1.8246	2.1206	2.1206
				0.5	1.2774	1.2774	−0.2292	−0.2292	0.5598	0.5598	0.5598	1.8464	1.8464	1.8292	1.8292

Table 2
Case I: descriptive quantities of motion for some values of c, c_1, c_2, c_3, and M^2.

M^2	c	c_1	c_2	c_3	$f''(0)$	$g''(0)$	$F'(0)$	$G'(0)$	h	α	β	$\overline{\eta}_f$	$\overline{\eta}_g$	$\overline{\eta}_F$	$\overline{\eta}_G$
1	−0.75	0.1	3.0	0.1	1.1976	0.4614	−0.0224	−0.0433	−1.8080	0.6867	1.5182	2.6606	4.4420	1.2244	0.9894
	−0.25	0.1	3.0	0.1	1.2091	0.9168	−0.0367	−0.0438	0.5981	0.6665	0.8716	2.4862	3.0164	1.1615	0.9980
	0.25	0.1	3.0	0.1	1.2445	1.2464	−0.0444	−0.0451	0.6276	0.6230	0.6459	2.2146	2.2937	1.0270	0.9997
	1.00	0.1	3.0	0.1	1.3139	1.6307	−0.0514	−0.0473	0.5272	0.5608	0.4935	1.8986	1.7754	0.8585	0.9722
5	−0.75	0.1	3.0	0.1	1.1468	1.9911	−0.0532	−0.0415	1.5051	0.7605	0.5124	3.1253	2.3336	0.7609	0.9647
	−0.25	0.1	3.0	0.1	1.1979	2.1699	−0.0560	−0.0434	0.7560	0.6784	0.4456	2.5426	1.9112	0.7170	0.9995
	0.25	0.1	3.0	0.1	1.2526	2.3362	−0.0582	−0.0453	0.5731	0.6164	0.4000	2.1889	1.6579	0.6640	0.9960
	1.00	0.1	3.0	0.1	1.3359	2.5665	−0.0608	−0.0479	0.4501	0.5479	0.3523	1.8557	1.4165	0.5817	0.9585

As one can see,

$$\lim_{\eta\to+\infty} f''(\eta) = 0, \qquad \lim_{\eta\to+\infty} f'(\eta) = 1, \qquad \lim_{\eta\to+\infty} f(\eta) - \eta = -\alpha.$$

As far as the behaviour of g, g', g'' is concerned, if $c < c_r$ (reverse flow appears) then it is shown in Fig. 6_1, otherwise it is given in Fig. 6_2.

Moreover, we have found a new interesting result: the function F presents a zone of reverse microrotation for some negative values of c. If $c < c_{rw}$ ($F'(0) > 0$) then the behaviour of F, F' is shown in Fig. 7_1, otherwise it is given in Fig. 7_2.

We underline that the thickness of the reverse microrotation zone is very small.

Fig. 8 shows the profiles of G, G'.

Table 2 shows the behaviour of the descriptive quantities of motion when M^2 and c change. We remark that in this table we consider only $c_1 = 0.1, c_2 = 3.0, c_3 = 0.1$ because the influence of these three parameters on the solution is the same as in the absence of the external magnetic field.

If M^2 increases, then $g''(0)$ increases, while $F'(0), \beta, \overline{\eta}_g, \overline{\eta}_F$ decrease. $G'(0), h, \alpha, \overline{\eta}_f, \overline{\eta}_G$ increase if $c < 0$, otherwise they decrease, and $f''(0)$ increases if $c > 0$, otherwise it decreases.

Further we underline that the thickness $\delta = (\overline{\eta}_f, \overline{\eta}_g, \overline{\eta}_F, \overline{\eta}_G)$ of the boundary layer depends on M^2 and decreases when M^2 increases (as easily seen in Figs. 9 and 10). This effect is standard in magnetohydrodynamics.

As it was underlined at the beginning of the Section 3, the magnetic field tends to prevent the occurrence of the reverse flow. So Tables 3 and 4 show that as the Hartmann number M^2 increases, the values of c_r and of c_{rw} for the reverse flow

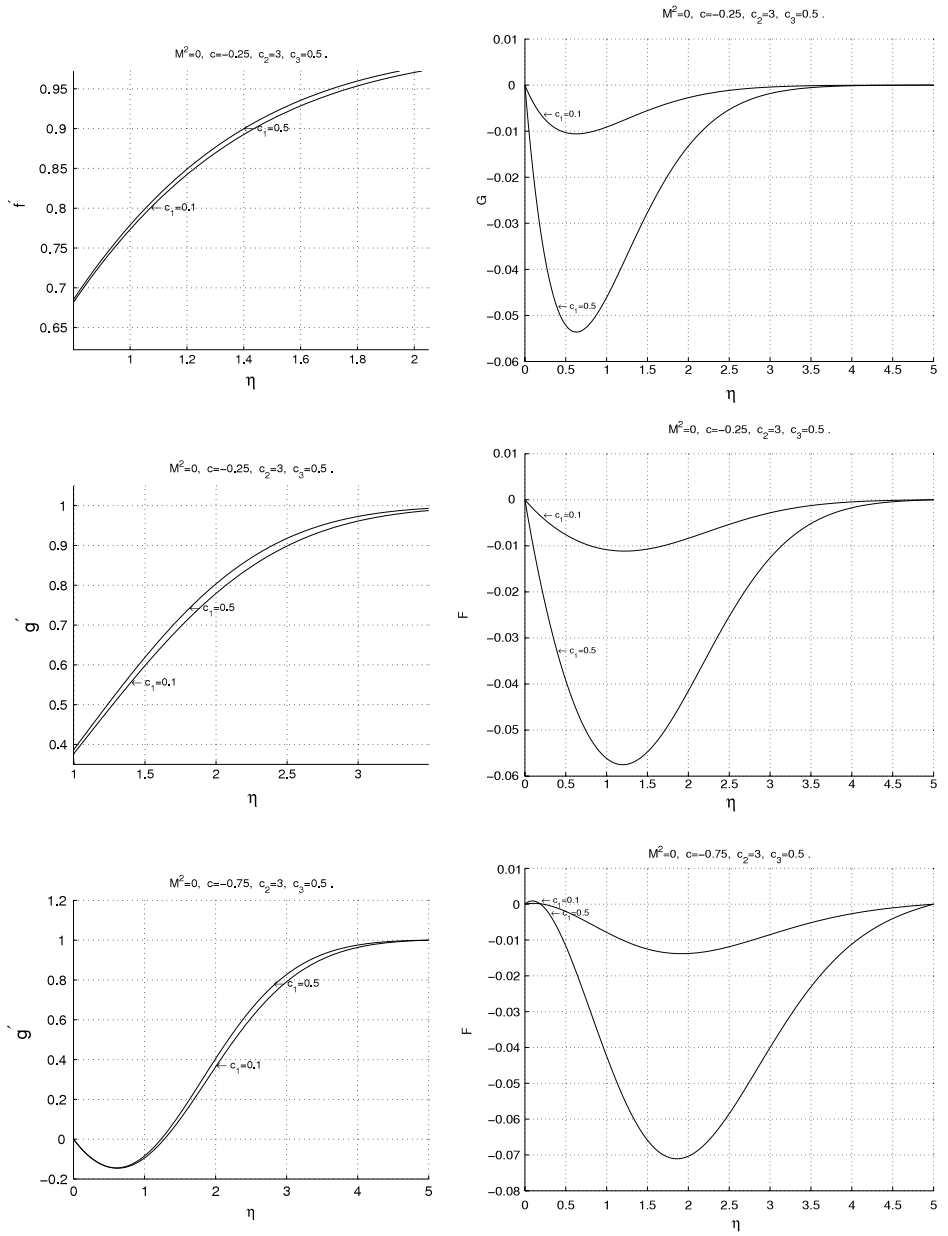

Fig. 2. f', g', F, G profiles for $M^2 = 0$, $c_2 = 3$, $c_3 = 0.5$ when $c_1 = 0.1$ and $c_1 = 0.5$. In the first four pictures $c = -0.25$ and there are not reverse flow and reverse microrotation. The last two pictures show the behaviour of g' and F with respect to c_1 when the reverse flow and the reverse microrotation occur ($c = -0.75$).

and the reverse microrotation decrease. In particular from $M^2 = 0.7810$ ($M^2 = 0.5148$), the reverse flow (the reverse microrotation) does not occur at all for any value of c. This fact could be explained by observing that $\frac{\partial p}{\partial x_3} = -\rho a^2 c x_3 (c + M^2)$ from which one can see that the signs of c and of $(c + M^2)$ modify the sign of $\frac{\partial p}{\partial x_3}$.

3.3. Case II: $\mathbf{H}_0 = H_0 \mathbf{e}_2$

The external magnetic field influences directly the velocity through the presence of M^2 in Eq. (13).

We have solved problem (13), (10), (11) numerically.

The behaviour of $f, f', f'', g, g', g'', F, F', G, G'$ is the same as in Case I. In particular, when $c < c_r$ the reverse flow appears and the behaviour of g, g', g'' is shown in Fig. 11_1. Moreover the function F presents a zone of reverse microrotation for some negative values of c. If $c < c_{rw}$ then the behaviour of F, F' is shown in Fig. 11_2.

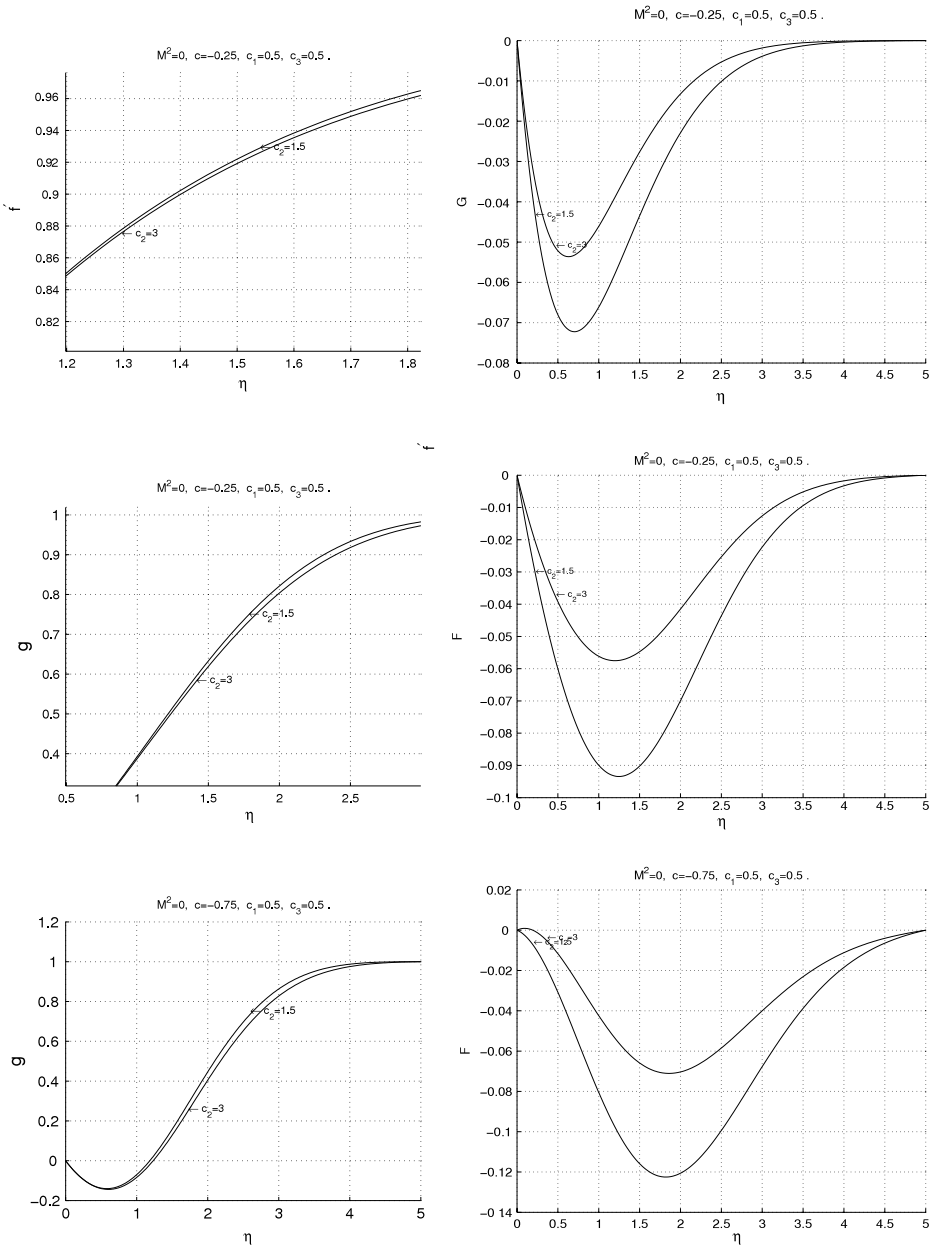

Fig. 3. f', g', F, G profiles for $M^2 = 0$, $c_1 = 0.5$, $c_3 = 0.5$ when $c_2 = 1.5$ and $c_2 = 3$. In the first four pictures $c = -0.25$ and there are not reverse flow and reverse microrotation. The last two pictures show the behaviour of g' and F with respect to c_2 when the reverse flow and the reverse microrotation occur ($c = -0.75$).

We refer to Figs. 5, 6_2, 7_2, 8 for the solution in the absence of reverse flow and reverse microrotation.

The values of the descriptive quantities of the motion are listed in Table 5 when M^2 and c change.

We notice that if M^2 is fixed, then the descriptive quantities of motion behave as in Case I when c increases.

When c, c_1, c_2, c_3 are fixed, from Table 5 we find that if M^2 increases, then $f''(0)$, $g''(0)$, $|F'(0)|$, $|G'(0)|$ increase, while the other parameters decrease.

Hence the thickness δ of the boundary layer depends on M^2 and decreases when M^2 increases (as easily seen in Figs. 12 and 13). We underline that in this case the boundary layer is thinner than in Case I.

Tables 6 and 7 show that as the Hartmann number M^2 increases, the values of c_r and of c_{rw} for the reverse flow and the reverse microrotation decrease. In particular from $M^2 = 0.7615$ ($M^2 = 0.4903$), the reverse flow (the reverse microrotation) does not occur at all for any value of c. Hence the magnetic field tends to prevent the occurrence of the

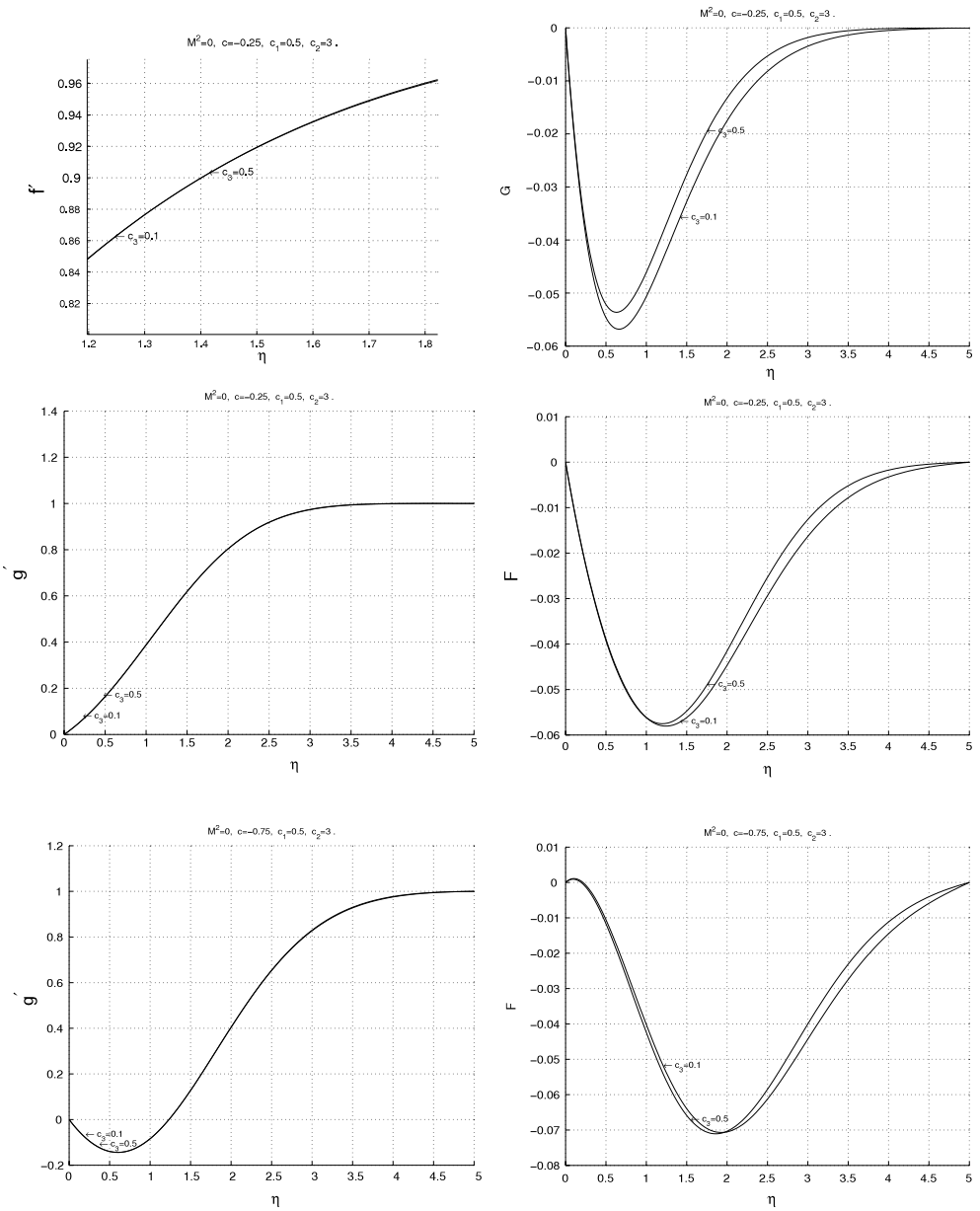

Fig. 4. f', g', F, G profiles for $M^2 = 0$, $c_1 = 0.5$, $c_2 = 3$ when $c_3 = 0.1$ and $c_3 = 0.5$. In the first four pictures $c = -0.25$ and there are not reverse flow and reverse microrotation. The last two pictures show the behaviour of g' and F with respect to c_3 when the reverse flow and the reverse microrotation occur ($c = -0.75$).

Table 3
Case I: values c_r when M^2 increases ($c_1 = 0.1, c_2 = 3.0, c_3 = 0.1$).

M^2	c_r
0.00	−0.4286
0.10	−0.4989
0.20	−0.5697
0.30	−0.6412
0.40	−0.7136
0.50	−0.7869
0.60	−0.8615
0.70	−0.9374
0.7809	−0.9999
0.7810	No reverse flow

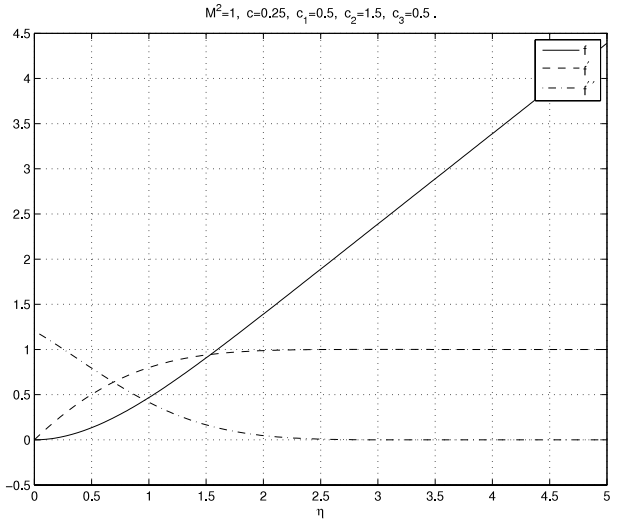

Fig. 5. Case I: f, f', f'' profiles.

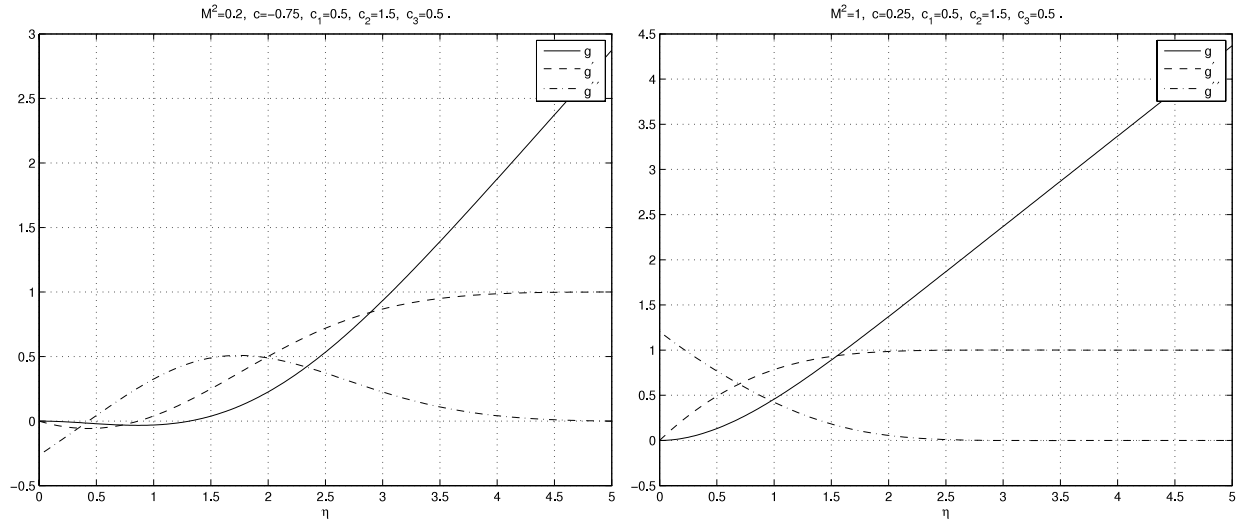

Fig. 6. Case I: The first picture shows the profiles of g, g', g'' in the reverse flow. The second picture shows the profiles of g, g', g'' in the absence of the reverse flow.

Table 4
Case I: values c_{rw} when M^2 increases ($c_1 = 0.1$, $c_2 = 3.0$, $c_3 = 0.1$).

M^2	c_{rw}
0.00	−0.6428
0.10	−0.7116
0.20	−0.7805
0.30	−0.8497
0.40	−0.9192
0.50	−0.9895
0.5147	−0.9999
0.5148	No reverse microrotation

reverse flow. In this case $\frac{\partial p}{\partial x_3} = -\rho a^2 c x_3 (c + 2M^2)$ from which one can see that the signs of c and of $(c + 2M^2)$ modify the sign of $\frac{\partial p}{\partial x_3}$.

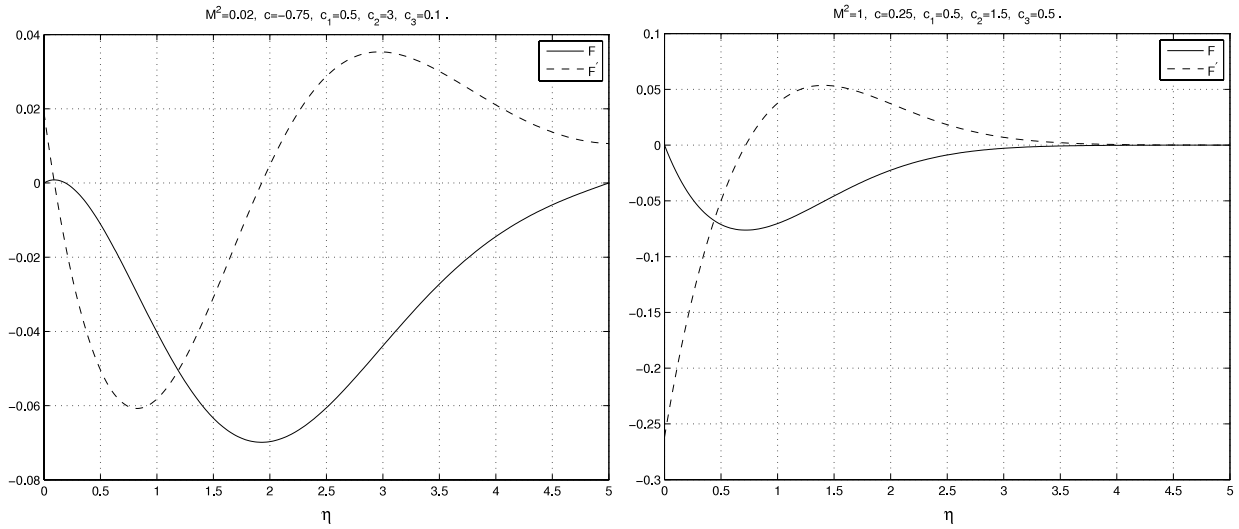

Fig. 7. Case I: the first picture shows the profiles of F, F' in the reverse microrotation. The second picture shows the profiles of F, F' in the absence of the reverse microrotation.

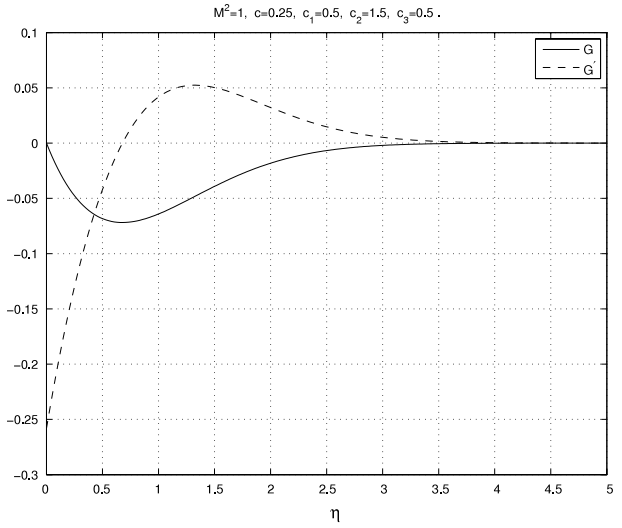

Fig. 8. Case I: G, G' profiles.

Table 5
Case II: descriptive quantities of motion for some values of c, c_1, c_2, c_3, and M^2.

M^2	c	c_1	c_2	c_3	$f''(0)$	$g''(0)$	$F'(0)$	$G'(0)$	h	α	β	$\overline{\eta}_f$	$\overline{\eta}_g$	$\overline{\eta}_F$	$\overline{\eta}_G$
1	−0.75	0.1	3.0	0.1	1.5603	0.4847	−0.0236	−0.0491	−2.0850	0.5607	1.4425	2.2677	4.3453	1.1640	0.8639
	−0.25	0.1	3.0	0.1	1.5677	0.9328	−0.0373	−0.0494	0.4514	0.5503	0.8470	2.1661	2.9329	1.1634	0.8677
	0.25	0.1	3.0	0.1	1.5905	1.2574	−0.0448	−0.0501	0.5486	0.5268	0.6358	1.9894	2.2541	1.0224	0.8687
	1.00	0.1	3.0	0.1	1.6378	1.6378	−0.0516	−0.0516	0.4895	0.4895	0.4895	1.7582	1.7582	0.8549	0.8549
5	−0.75	0.1	3.0	0.1	2.5220	2.0106	−0.0538	−0.0597	0.0316	0.3786	0.4943	1.6646	2.1937	0.7644	0.5850
	−0.25	0.1	3.0	0.1	2.5359	2.1870	−0.0564	−0.0601	0.3482	0.3697	0.4345	1.5766	1.8339	0.7145	0.5855
	0.25	0.1	3.0	0.1	2.5519	2.3512	−0.0586	−0.0605	0.3671	0.3608	0.3925	1.4954	1.6094	0.6597	0.5837
	1.00	0.1	3.0	0.1	2.5788	2.5788	−0.0611	−0.0611	0.3477	0.3477	0.3477	1.3885	1.3885	0.5770	0.5770

We point out that the values of M^2 starting from which the reverse flow and the reverse microrotation do not appear for any values of c are smaller than in Case I.

3.4. *Case III:* $\mathbf{H}_0 = H_0\mathbf{e}_3$

The external magnetic field influences directly the velocity through M^2 which appears only in Eq. $(14)_1$.

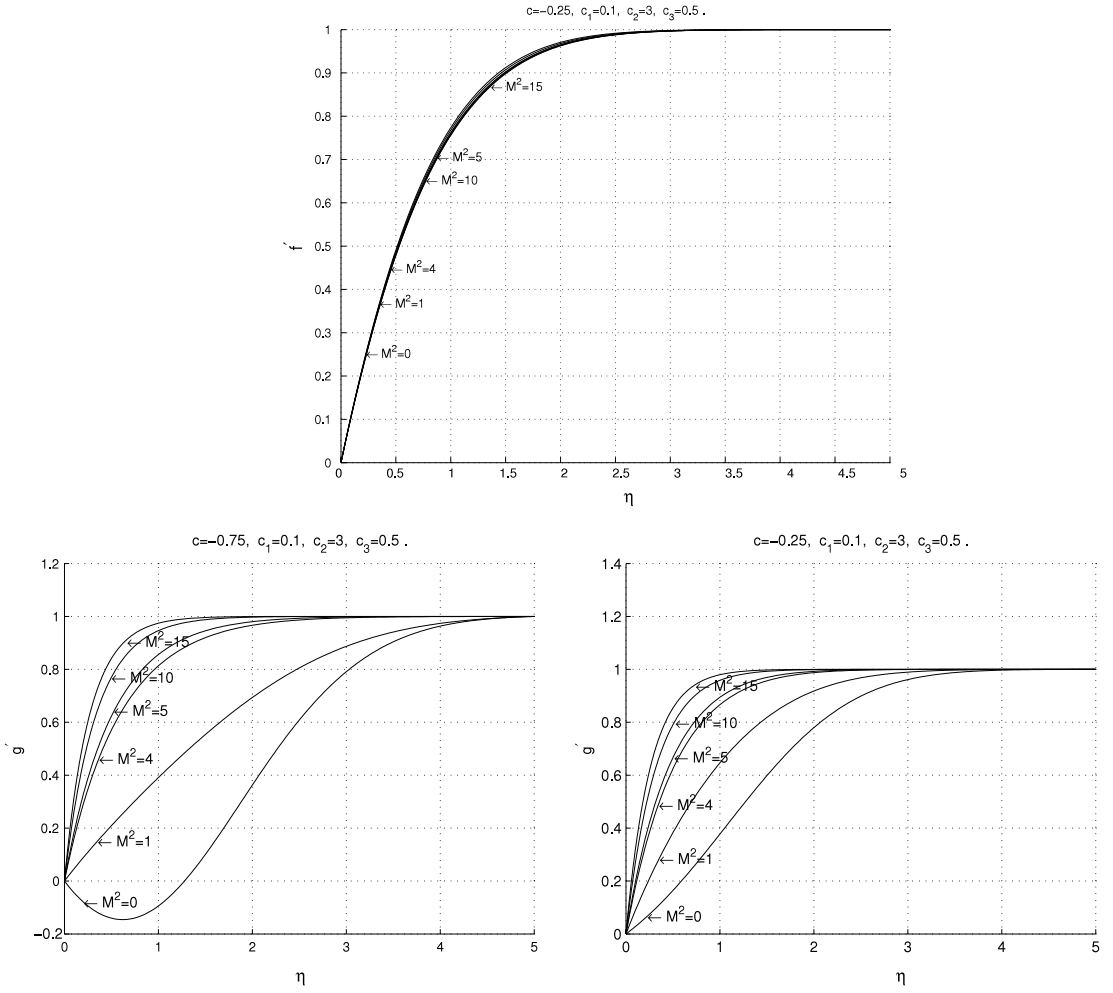

Fig. 9. Case I: profiles of f' (9_1) and g' ($9_{2,3}$) for several values of M^2 which elucidate the boundary layer thickness.

Table 6
Case II: values c_r when M^2 increases ($c_1 = 0.1, c_2 = 3.0, c_3 = 0.1$).

M^2	c_r
0.00	−0.4286
0.10	−0.5022
0.20	−0.5759
0.30	−0.6499
0.40	−0.7244
0.50	−0.7994
0.60	−0.8753
0.70	−0.9521
0.7614	−0.9999
0.7615	No reverse flow

We have solved problem (14), (10), (11) numerically.

Fig. 14_1 shows the graphics of g, g', g'' when $c < c_r$ (reverse flow), while we display the profiles of F, F' when $c < c_{rw}$ in 14_2 (reverse microrotation).

We refer to Figs. 5, 6_2, 7_2, 8 for the behaviour of the solution in the absence of reverse flow and reverse microrotation.

In Table 8 we give the values of the descriptive quantities of motion when M^2 and c change.

We notice that if M^2 is fixed, then the descriptive quantities behave as in CASEs I–II when c increases.

When c, c_1, c_2, c_3 are fixed, from Table 8 we find that if M^2 increases, then $f''(0)$, $|g''(0)|$, $|F'(0)|$, $|G'(0)|$ increase, while the other parameters decrease.

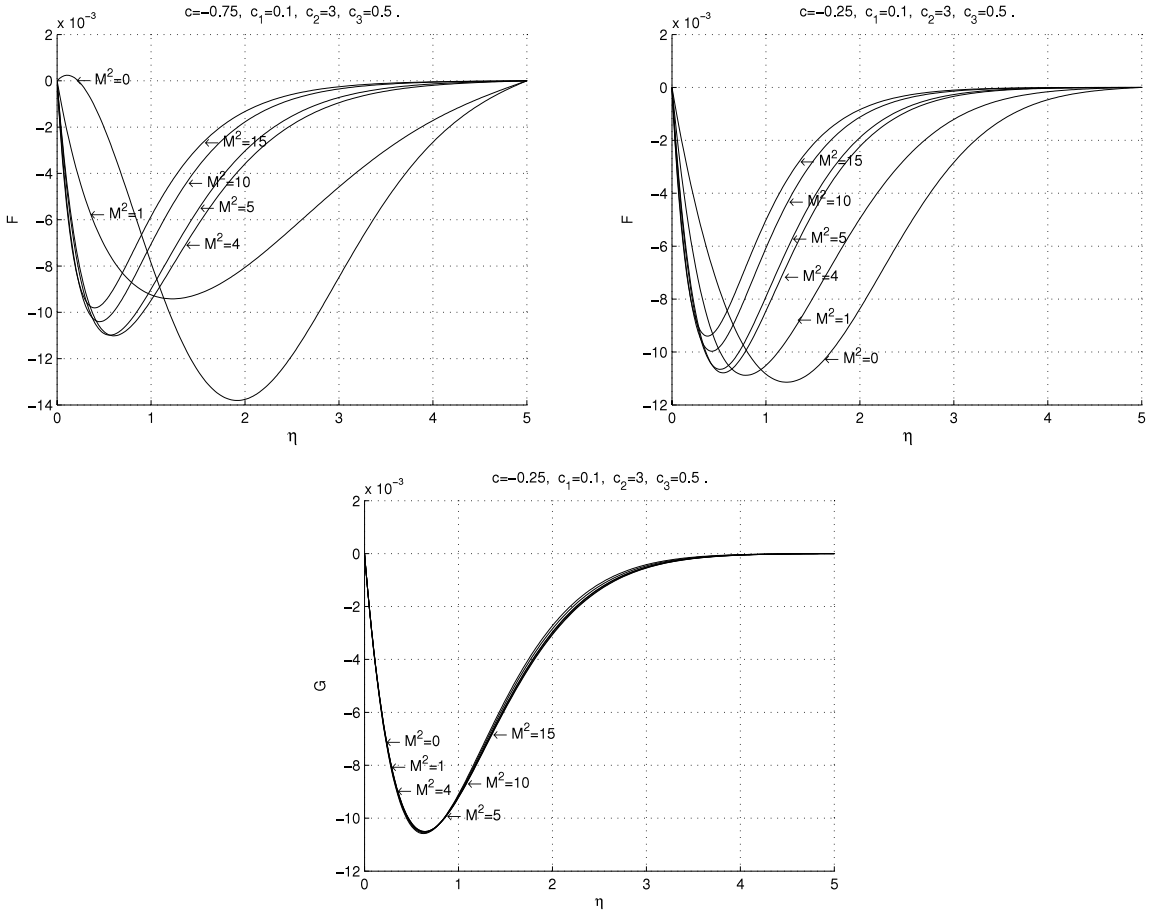

Fig. 10. Case I: profiles of F ($10_{1,2}$) and G (10_3) for several values of M^2 which elucidate the boundary layer thickness.

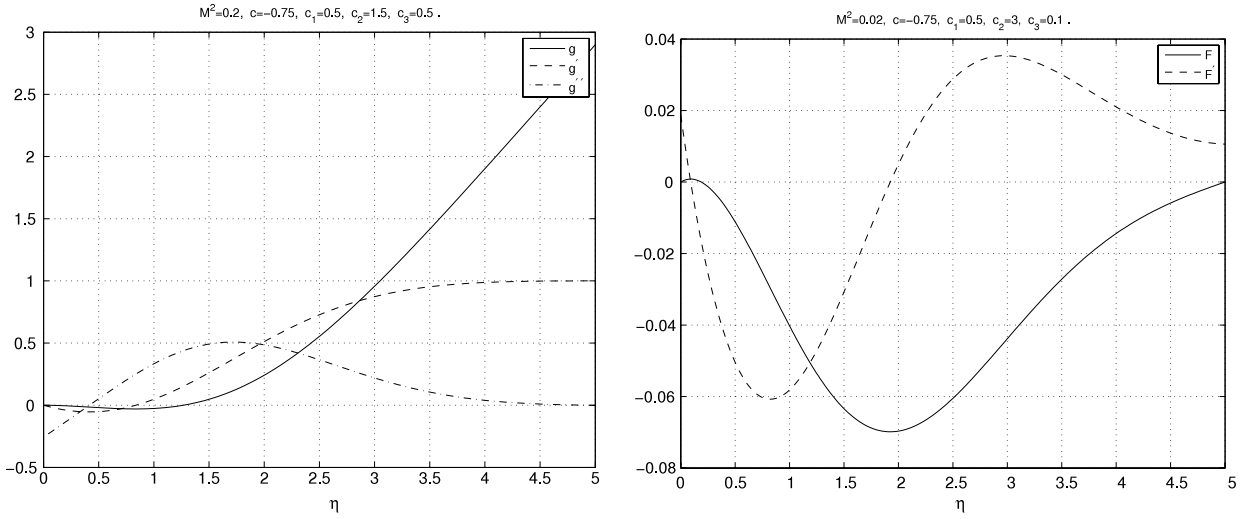

Fig. 11. Case II: the first picture shows the profiles of g, g', g'' in the reverse flow. The first picture shows the profiles of F, F' in the reverse microrotation.

Hence the thickness δ of the boundary layer depends on M^2 and decreases when M^2 increases (as easily seen in Figs. 15 and 16). We underline that the boundary layer in Case II is thinner than in this case.

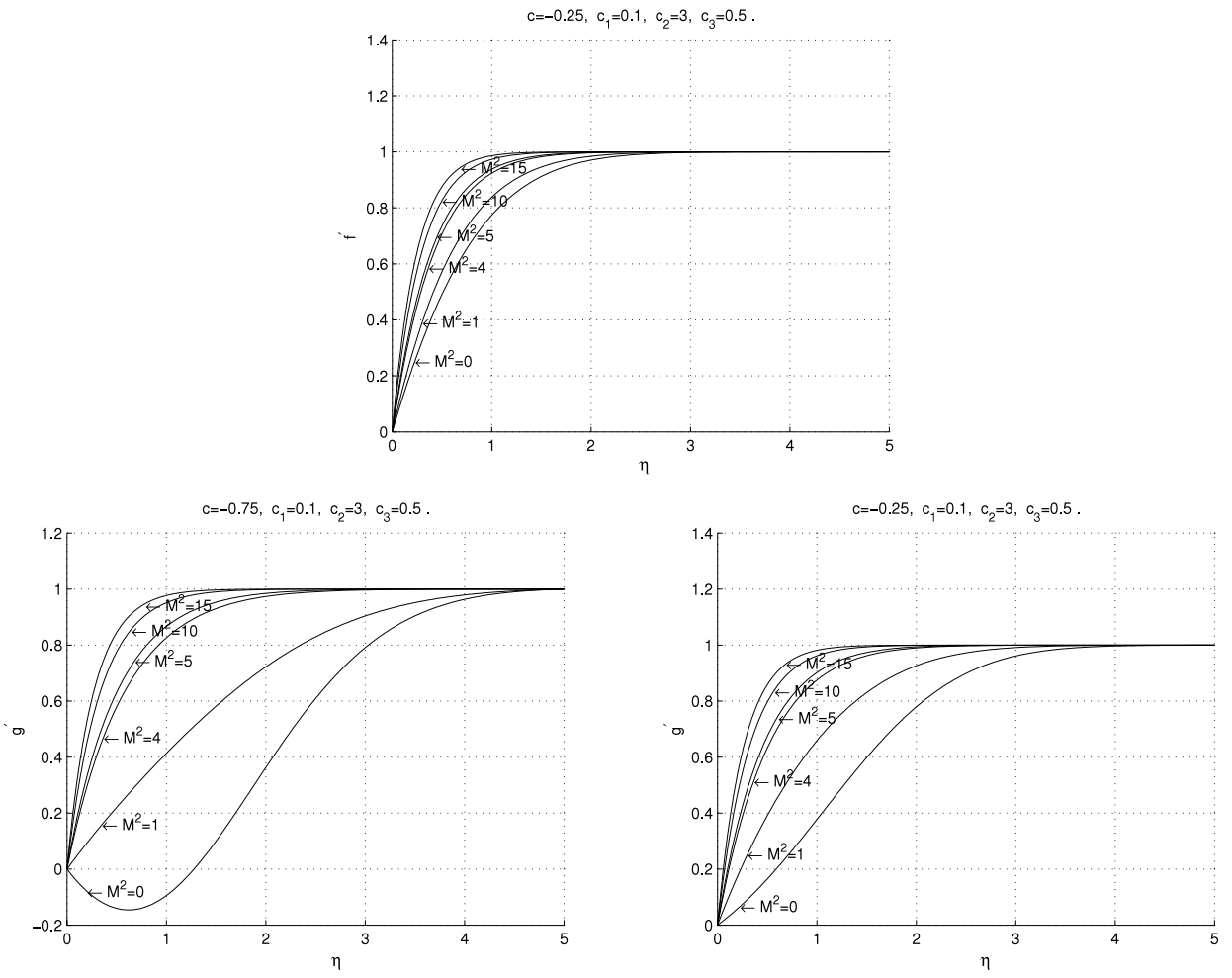

Fig. 12. Case II: profiles of f' (12_1) and g' ($12_{2,3}$) for several values of M^2 which elucidate the boundary layer thickness.

Table 7
Case II: values c_{rw} when M^2 increases ($c_1 = 0.1, c_2 = 3.0, c_3 = 0.1$).

M^2	c_{rw}
0.00	−0.6428
0.10	−0.7162
0.20	−0.7891
0.30	−0.8617
0.40	−0.9343
0.4902	−0.9999
0.4903	No reverse microrotation

Table 8
Case III: descriptive quantities of motion for some values of c, c_1, c_2, c_3, and M^2.

M^2	c	c_1	c_2	c_3	$f''(0)$	$g''(0)$	$F'(0)$	$G'(0)$	h	α	β	$\overline{\eta}_f$	$\overline{\eta}_g$	$\overline{\eta}_F$	$\overline{\eta}_G$
1	−0.75	0.1	3.0	0.1	1.5865	−0.4357	0.0033	−0.0500	−5.1062	0.5339	2.4140	2.0722	4.4471	2.8076	0.8650
	−0.25	0.1	3.0	0.1	1.5730	0.2990	−0.0221	−0.0495	0.2958	0.5453	1.2938	2.1332	3.4613	1.7201	0.8674
	0.25	0.1	3.0	0.1	1.5874	0.8165	−0.0369	−0.0500	0.5847	0.5291	0.8069	2.0017	2.5434	1.2509	0.8695
	1.00	0.1	3.0	0.1	1.6307	1.3139	−0.0473	−0.0514	0.5272	0.4935	0.5608	1.7754	1.8986	0.9722	0.8585
5	−0.75	0.1	3.0	0.1	2.5471	−0.3730	0.0002	−0.0604	−5.2656	0.3639	2.2405	1.5296	4.3655	2.6548	0.5839
	−0.25	0.1	3.0	0.1	2.5416	0.3618	−0.0247	−0.0602	0.0932	0.3668	1.1874	1.5522	3.2934	1.6262	0.5847
	0.25	0.1	3.0	0.1	2.5477	0.8531	−0.0382	−0.0604	0.4443	0.3627	0.7706	1.5089	2.4504	1.2210	0.5849
	1.00	0.1	3.0	0.1	2.5665	1.3359	−0.0479	−0.0608	0.4501	0.3523	0.5479	1.4165	1.8557	0.9585	0.5817

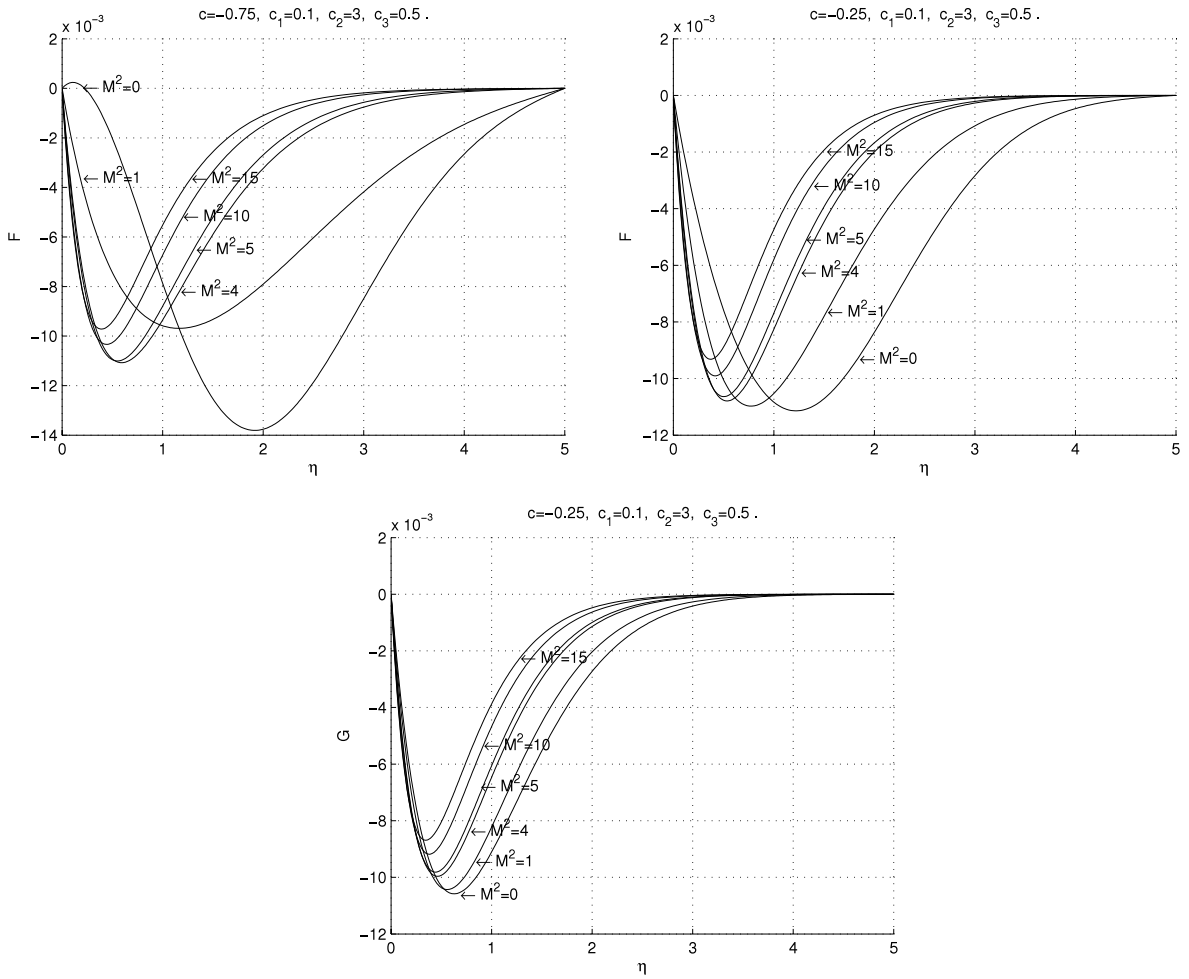

Fig. 13. Case II: profiles of F (13_1) and G ($13_{2,3}$) for several values of M^2 which elucidate the boundary layer thickness.

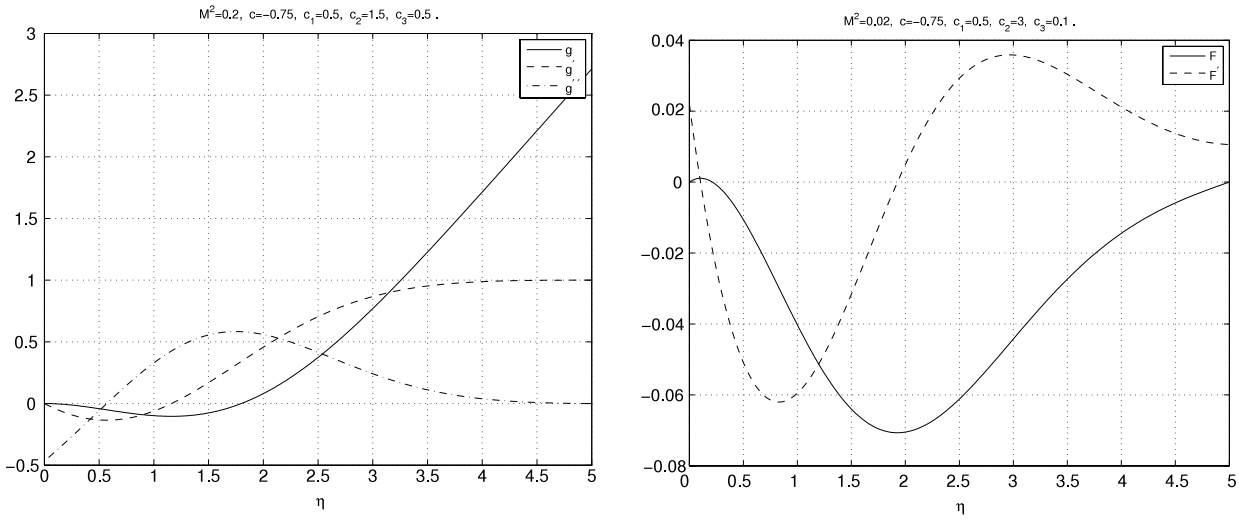

Fig. 14. Case III: the first picture shows the profiles of g, g', g'' in the reverse flow. The second picture shows the profiles of F, F' in the absence of the reverse microrotation.

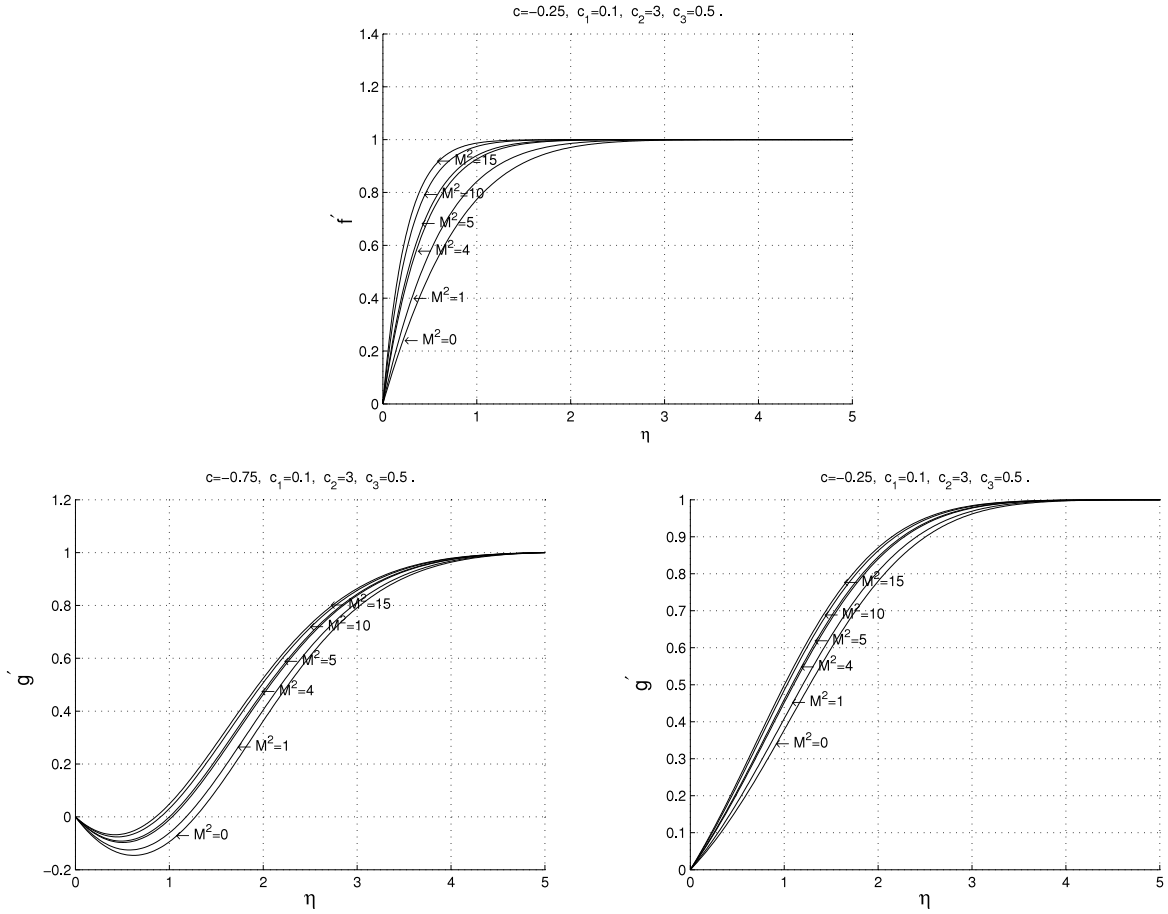

Fig. 15. Case III: profiles of f' (15_1) and g' ($15_{2,3}$) for several values of M^2 which elucidate the boundary layer thickness.

Table 9
Case III: values c_r when M^2 increases ($c_1 = 0.1, c_2 = 3.0, c_3 = 0.1$).

M^2	c_r
0.00	−0.4286
1.00	−0.4558
2.00	−0.4735
10.00	−0.5297
20.00	−0.5531
50.00	−0.5780
100.00	−0.5919

Tables 9 and 10 show that as the Hartmann number M^2 increases, the values of c_r and of c_{rw} decrease very slowly, so that in this case the influence of the magnetic field is much less significant with respect to CASEs I–II. In this regard we observe that $\frac{\partial p}{\partial x_3}$, $\frac{\partial p}{\partial x_1}$ have the same sign that they would have in the absence of the external magnetic field.

In particular, we see that the reverse flow and the reverse microrotation always appear for physically meaningful values of M^2.

4. Conclusions

A numerical study is performed for the steady three-dimensional MHD stagnation-point flow of an incompressible, homogeneous electrically conducting micropolar fluid over a flat plate in the presence of a uniform external magnetic field. The main advantage of using a micropolar fluid model to study this problem in comparison with other classes of non-Newtonian fluids is that it takes into account the rotation of fluid particles by means of an independent kinematic vector called the microrotation vector. This model is considered to describe, for example, biological fluids in thin vessels, polymeric suspensions, slurries, colloidal fluids.

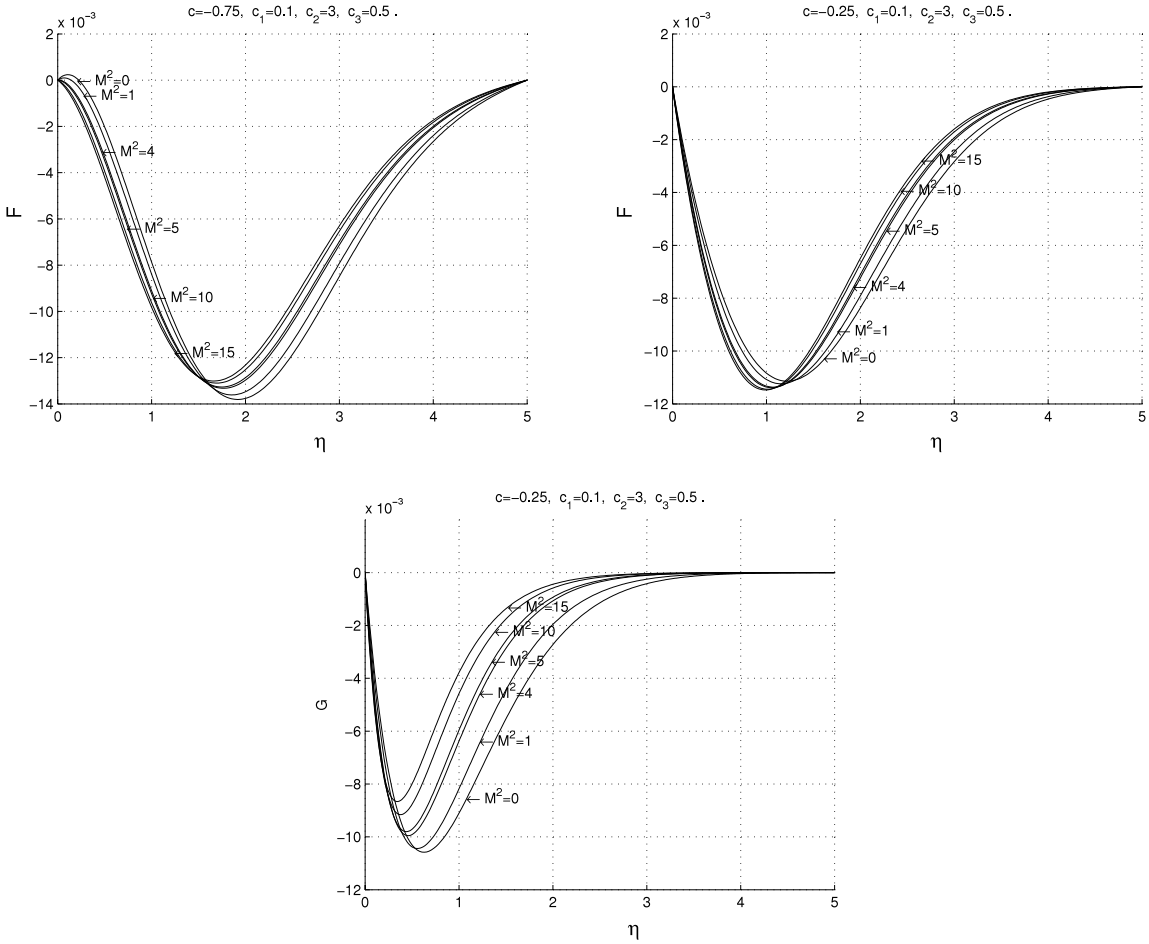

Fig. 16. Case III: profiles of F (16_1) and G ($16_{2,3}$) for several values of M^2 which elucidate the boundary layer thickness.

Table 10
Case III: values c_{rw} when M^2 increases ($c_1 = 0.1, c_2 = 3.0, c_3 = 0.1$).

M^2	c_{rw}
0.00	−0.6428
1.00	−0.6804
2.00	−0.7044
10.00	−0.7775
20.00	−0.8064
50.00	−0.8360
100.00	−0.8521

This paper completes our previous analysis for the micropolar fluids in [4], where we have proved that, if we impress an external magnetic field $\mathbf{H}_0$, and we neglect the induced magnetic field (as it is customary in the literature when the magnetic Reynolds number is very small), then the steady three-dimensional MHD stagnation-point flow is possible if, and only if, $\mathbf{H}_0$ has the direction of one of the coordinate axes.

In particular, we have solved numerically the three non-linear ordinary boundary value problems by using the MATLAB routine **bvp4c**.

The following conclusions can be made for the three cases considered.

- The presence of the magnetic field modifies the thickness δ of the boundary layer which decreases as M^2 increases.
- A new interesting result for some negative values of c has been observed for the microrotation: as well as for the velocity, the microrotation presents a zone of reverse microrotation, where $F'(0) > 0$.
- $\mathbf{H}_0$ tends to prevent the occurrence of the reverse flow and of the reverse microrotation in a relevant way in CASEs I–II.
- Analysing the values of c_r and c_{rw}, we can see that the range of c for which the reverse microrotation appears is included in the range of c for which the reverse flow occurs.

- The material micropolar parameters c_1, c_2, c_3 influence most the microrotation and c_1 is the parameter that affects most among c_1, c_2, c_3.
- The three-dimensional displacement thickness h can be positive or negative and it is always negative when the reverse flow appears.
- In Case II, δ and the values of M^2 starting from which the reverse flow and the reverse microrotation do not appear for any values of c are smaller than in the other cases.
- In the literature there are no papers concerning the influence of electromagnetic field on the three-dimensional stagnation-point flow of micropolar fluids. Our results are consistent with the previous studies when $M^2 = 0$ [21] and they extend them.

Moreover, it can be interesting to compare these results with the corresponding results for the Newtonian fluid [22]:

- the micropolar fluids reduce the thickness of the boundary layer.
- the presence of the microrotation decreases the values of $f''(0)$ and of $g''(0)$, so that the magnitude of the skin friction is smaller than that in the Newtonian case.
- if the fluid is micropolar, then in CASEs I–II when $M^2 > 0.2$, c_r is smaller.

As in the Newtonian case, for a micropolar fluid, the origin can be classified as nodal or saddle and as attachment or separation point: this classification depends on the values of $f''(0)$ and of $g''(0)$ and it is analogous to the analysis contained in [22].

As far as the applications are concerned, from a theoretical point of view, MHD flows of this type are fundamental in fluid dynamics. From a practical point of view, it may be noticed that stagnation-point flows are ubiquitous in the sense that they inevitably appear as a component of more complicated flow fields. So the investigation in this area is motivated by the possibility of solving exactly the boundary layer equations at the stagnation point and by their relevance to a wide range of engineering, industrial and technical applications.

Acknowledgements

The authors are grateful to the referees for the useful and valuable suggestions.

References

[1] F. Homman, Der Einfluss grosser Zahigkeit bei der Stromung um den Zylinder und um die Kugel, ZAMM Z. Angew. Math. Mech. 16 (1936) 153–164.
[2] L. Howarth, The boundary layer in three dimensional flow—Part II, the flow near a stagnation point, Phil. Mag. 7 (1951) 1433–1440.
[3] A. Davey, Boundary layer flow at a saddle point of attachment, J. Fluid Mech. 10 (1961) 593–610.
[4] A. Borrelli, G. Giantesio, M.C. Patria, Three-dimensional MHD stagnation point-flow of a Newtonian and a micropolar fluid, Int. J. Pure Appl. Math. 73 (2011) 165–188.
[5] A.C. Eringen, Microcontinuum Field Theories, Vol. I–II, Springer-Verlag, 2001.
[6] G. Lukaszewicz, Micropolar Fluids Theory and Applications, Birkäuser, 1999.
[7] F. Shahzad, M. Sajid, T. Hayat, M. Ayub, Analytic solution for flow a micropolar fluid, Acta Mech. 188 (2006) 93–102.
[8] T. Hayat, T. Javed, Z. Abbas, MHD flow of a micropolar fluid near a stagnation point towards a non-linear streching surface, Nonlinear Anal. Real World Appl. 10 (2009) 1514–1526.
[9] M. Sajid, Z. Abbas, T. Hayat, Homotopy analysis for boundary layer flow of a micropolar fluid through a porous channel, Appl. Math. Model. 33 (2009) 4120–4125.
[10] F. Xu, Regularity criterion of weak solution for the 3D Magneto-micropolar fluid equations in Besov spaces, Commun. Nonlinear Sci. Numer. Simul. 17 (2012) 2426–2433.
[11] T. Hayat, N. Ali, Z. Abbas, Peristaltic flow of a micropolar fluid in a channel with different wave forms, Phys. Lett. A 370 (2007) 331–344.
[12] T. Hayat, Z. Abbas, T. Javed, Mixed covection flow of a micropolar fluid over a non-linearly streching shit, Phys. Lett. A 372 (2008) 637–647.
[13] N. Ali, T. Hayat, Peristaltic flow of a micropolar fluid in a asymetric channel, Comput. Math. Appl. 55 (2008) 589–608.
[14] T. Hayat, N. Ali, Effects of an endoscope on peristaltic flow of a micropolar fluid, Math. Comput. Modelling 48 (2008) 721–733.
[15] M. Sajid, N. Ali, T. Hayat, On exact solutions for thin film flows of a micropolar fluid, Commun. Nonlinear Sci. Numer. Simul. 14 (2009) 451–461.
[16] A. Borrelli, G. Giantesio, M.C. Patria, MHD oblique stagnation-point flow of a micropolar fluid, Appl. Math. Model. 36 (2012) 3949–3970.
[17] A.M. Abd-Alla, G.A. Yahya, S.R. Mahmoud, H.S. Alosaimi, Effect of the rotation, magnetic field and initial stress on peristaltic motion of micropolar fluid, Meccanica 47 (2012) 1455–1465.
[18] M. Ashraf, S. Bashir, Numerical simulation of MHD stagnation point flow and heat transfer of a micropolar fluid towards a heated shrinking sheet, Internat. J. Numer. Methods Fluids 69 (2012) 384–398.
[19] M.A.A. Mahmoud, S.E. Waheed, MHD stagnation point flow of a micropolar fluid towards a moving surface with radiation, Meccanica 47 (2012) 1119–1130.
[20] G. Ahmadi, Self-Similar solution of incompressible micropolar boundary layer flow over a semi-infinite plate, Internat. J. Engrg. Sci. 10 (1976) 639–646.
[21] G.S. Guram, M. Anwar Kamal, Three-dimensional micropolar flow near saddle and nodal points of attachment, Comput. Math. Appl. 22 (1991) 1–9.
[22] A. Borrelli, G. Giantesio, M.C. Patria, On the numerical solutions of three-dimensional MHD stagnation-point flow of a Newtonian fluid, IJPAM (2013) (in press).
[23] P. Drazin, N. Riley, The Navier–Stokes Equations. A Classification of Flows and Exact Solutions, in: London Mathematical Society, Lecture Notes Series, vol. 334, Cambridge University Press, 2007.
[24] L.F. Shampine, I. Gladwell, S. Thompson, Solving ODEs with MATLAB, Cambridge University Press, 2003.
[25] A. Davey, Rotational flow near a forward stagnation point, Quart. J. Mech. Appl. Math. 26 (1963) 33–59.
[26] S. Bhattacharyya, A.S. Gupta, MHD flow and heat transfer at a general three-dimensional stagnation point, Int. J. Non-Linear Mech. 33 (1998) 125–134.